Article
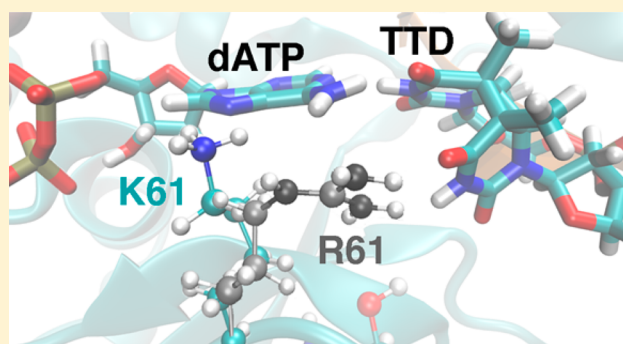
Effects of Active Site Mutations on Specificity of Nucleobase Binding in Human DNA Polymerase η

Melek N. Ucisik and Sharon Hammes-Schiffer*

Department of Chemistry, University of Illinois at Urbana-Champaign, 600 South Mathews Avenue, Urbana, Illinois 61801-3364, United States

S Supporting Information

ABSTRACT: Human DNA polymerase η (Pol η) plays a vital role in protection against skin cancer caused by damage from ultraviolet light. This enzyme rescues stalled replication forks at cyclobutane thymine−thymine dimers (TTDs) by inserting nucleotides opposite these DNA lesions. Residue R61 is conserved in the Pol η enzymes across species, but the corresponding residue, as well as its neighbor S62, is different in other Y-family polymerases, Pol ι and Pol κ. Herein, R61 and S62 are mutated to their Pol ι and Pol κ counterparts. Relative binding free energies of dATP to mutant Pol η•DNA complexes with and without a TTD were calculated using thermodynamic integration. The binding free energies of dATP to the Pol η•DNA complex with and without a TTD are more similar for all of these mutants than for wild-type Pol η, suggesting that these mutations decrease the ability of this enzyme to distinguish between a TTD lesion and undamaged DNA. Molecular dynamics simulations of the mutant systems provide insights into the molecular level basis for the changes in relative binding free energies. The simulations identified differences in hydrogen-bonding, cation−π, and π−π interactions of the side chains with the dATP and the TTD or thymine−thymine (TT) motif. The simulations also revealed that R61 and Q38 act as a clamp to position the dATP and the TTD or TT and that the mutations impact the balance among the interactions related to this clamp. Overall, these calculations suggest that R61 and S62 play key roles in the specificity and effectiveness of Pol η for bypassing TTD lesions during DNA replication. Understanding the basis for this specificity is important for designing drugs aimed at cancer treatment.

1. INTRODUCTION

Ultraviolet (UV) light from the sun is one of the most common causes of DNA lesions. The enzyme DNA polymerase η (Pol η), which is a Y-family DNA polymerase, plays a critical role in allowing the human body to tolerate this type of damage.[1] The lack or malfunction of human Pol η as a result of mutations of the gene encoding leads to the variant form of Xeroderma Pigmentosum, a disease entailing intolerance to UV-induced skin damage and elevated predisposition to skin cancer.[2] Pol η performs translesion synthesis[3] to rescue stalled replication forks due to the presence of cyclobutane pyrimidine dimers, specifically cis−syn cyclobutane thymine−thymine dimers (TTDs), which cannot be handled by replicative DNA polymerases α, δ, and ε.[4,5] Pol η exhibits a relatively high accuracy and processivity at lesion sites,[6,7] while its overall efficiency and fidelity decrease in the absence of a lesion in the template DNA strand.[8] Pol η also targets the DNA adducts of Pt-based chemotherapy agents such as cisplatin, oxaliplatin, and gemcitabine, and its action at the sites of these anticancer agents reduces their potency.[9−11] Thus, understanding the basis of the processivity and selectivity of Pol η is important for preventing its interference with cancer chemotherapy.

Our previous work provided some structural and thermodynamic insights into the binding properties of various Pol η-DNA systems.[12,13] Herein, we investigate the effects of active site mutations of residues R61 and S62 on two Pol η-DNA systems, one with a TTD lesion in its template DNA and one without this lesion. This work aims to elucidate the contributions of these residues, which differ across the Y-family DNA polymerases, to the specificity of Pol η. The sites of mutation were chosen by superimposing the active sites of Pol η onto two other Y-family human DNA polymerases, Pol ι[14] and Pol κ.[15−17] Pol ι is suggested to have evolved from Pol η by a gene duplication,[18,19] although it is very different from Pol η and other Y-family DNA polymerases in terms of its biochemical function. Pol ι can use noncanonical Hoogsteen interactions in nucleotide base pairing, which might play a significant role in replication of various types of DNA lesions impairing Watson−Crick base pairing.[14] Pol κ is implicated in the extension step of the translesion bypass[16] and is specialized

in handling bulky DNA minor groove lesions.[5,15] The wide variety of DNA lesions that must be countered requires specialized DNA polymerases, which mostly share a common active site scaffold and sequence. The diversity in their functions appears to arise from differences in only a few active site residues.

The alignment of Pol η, Pol ι, and Pol κ indicates that, out of 14 residues in the active site, only those corresponding to F18, I48, R61, and S62 of Pol η are different across these three polymerases (Figure S1, Table S1). Because the interactions of the residues at the F18 and I48 sites with the incoming deoxyadenosine triphosphate (dATP) are through their backbone atoms, exchanging them with a different amino acid would not be expected to significantly affect the interactions within the active site. Thus, we chose to mutate R61 and S62 in Pol η to their Pol ι and Pol κ counterparts. Specifically, R61 was mutated to K and A, while S62 was mutated to L and A.

R61 was found to be one of the two conserved residues in the Pol η enzymes across species.[20] Previously, its mutation to an Ala was found to reduce the experimentally measured polymerase efficiency (k_{cat}/K_M) for adenine incorporation opposite a template thymine (T) in a Pol η•TTD-containing DNA complex.[20] It was also hypothesized that the positioning and the positive charge of R61 contribute to the activity of Pol η in the context of another abundant DNA lesion, 7,8-dihydro-8-oxo-2′-deoxyguanosine (8-oxoG).[21] In our recent molecular dynamics (MD) studies of wild-type (WT) Pol η,[12] we observed persistent cation−π interactions[22,23] between R61 and the incoming dATP. Additionally, somewhat less persistent hydrogen-bonding interactions were observed between its guanidinium hydrogens and the nitrogen or oxygen atoms of the dATP.[12] Moreover, a recent computational study suggests that certain conformations of R61 assist in the recruitment of the incoming dATP and facilitate both the formation of a prereactive complex in Pol η for efficient damage bypass and the expulsion of the leaving pyrophosphate of dATP after the nucleotidyl addition reaction.[24] A more recent computational study has also investigated the mechanism for Pol η using mixed quantum mechanical/molecular mechanical methods.[25]

In this paper, we present relative binding free energies of dATP to a mutant Pol η complexed with a DNA template−primer pair either with or without a TTD. These binding free energies are calculated with the thermodynamic integration (TI) method. For the reasons discussed above, the mutants examined were R61K, R61A, S62L, and S62A. To gain atomic-level insights into the calculated relative binding free energies from the TI calculations, we also performed extensive molecular dynamics (MD) simulations on each mutant system complexed with DNA containing either a TTD or a TT motif. Our analysis provides insights into key interactions that impact the efficiency and specificity of Pol η.

2. METHODS

We calculated relative binding free energies of dATP to the catalytic core of Pol η, which is comprised of 432 amino acid residues and two Mg^{2+} ions required for the nucleotidyl addition reaction,[20] complexed with a DNA template−primer pair either with or without a TTD. We performed these calculations for a series of Pol η mutants using TI. In each of the thermodynamic cycles used for this purpose, one of the following mutations was performed on the crystal structure 3MR3:[20] R61K, R61A, S62L, or S62A. Additionally, extensive

molecular dynamics (MD) simulations were conducted on the mutant systems with either a TTD or a TT motif.

In all of our calculations, the solute and solvent atoms were treated explicitly using the ff12SB force field[26−29] for the protein, the ff99bsc0 force field for the DNA, and TIP3P water[30] within the AMBER14 suite of programs.[31] The Mg^{2+} parameters employed were from Allner et al.[32] The Mg^{2+} ions retained their original crystal structure positions throughout the simulations, although they were allowed to move freely. The atomic charges for the TTD and dATP were obtained using the restrained electrostatic potential (RESP) method.[33,34] The detailed protocol used to determine these charges, as well as the specific atomic charges, is described elsewhere.[12] In all of these simulations, the SHAKE algorithm[35] was employed to constrain covalent bonds involving hydrogen, and the particle mesh Ewald (PME) method[36] was used for long-range electrostatic interactions with a 12 or 8 Å nonbonded cutoff to limit the direct space sum for the TI and MD simulations, respectively. A time step of 2 fs was employed for all simulations.

The starting structures for the free energy calculations and the MD simulations of the mutant systems were extracted from MD trajectories[12] performed on a complex of the WT Pol η catalytic core, dATP, and a DNA template−primer either with or without a TTD based on the crystal structure 3MR3[20] or 3MR2,[20] respectively. The extracted configurations were subjected to a point mutation at the residue numbered 61 or 62. Residue 61 was mutated from R to K or A, and residue 62 was mutated to L or A. These specific mutations were chosen by superimposing the 3MR3[20] Pol η crystal structure with the crystal structures of Pol ι (PDB ID: 3OSN[37]) and Pol κ (PDB ID: 2W7O[38]), which are also Y-family polymerases. This alignment identified residues 61 and 62 as the key differences (Table S1) in terms of residues in which the amino acid side chains interact with the dATP. Thus, in our mutation studies, these residues were replaced with their Pol ι and Pol κ counterparts. The mutations were incorporated by keeping the highest possible number of the original side chain atoms, namely, those of R61 or S62, as part of the new side chain, followed by the geometry optimization mentioned below. After incorporation of the new side chain atoms, the systems were neutralized with the addition of Na^+ ions, solvated with a periodically replicated octahedral TIP3P[30] triangulated water box with sides at least 10 Å from any solute atom, and buffered by adding ~125 mM NaCl. The charged amino acids were simulated in their protonation states obtained with the H++ protonation state web server at neutral pH.[39] Directly following this system preparation, the mutated residues were energy-minimized while all other atoms were kept stationary with harmonic restraints.

The TI calculations used the pmemd implementation[40] of alchemical transformations in the AMBER 14 suite.[31] The thermodynamic cycle used for the TI calculations is shown in Scheme 1. The difference in binding free energies of dATP to a

Scheme 1. Thermodynamic Cycle Used for Calculating Relative Binding Free Energies of dATP to a Complex of Mutated Pol η and TTD- or TT-Containing DNA
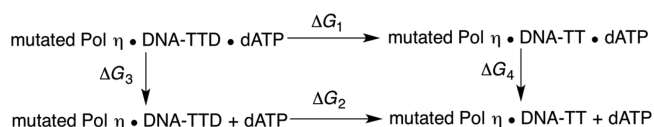
complex comprised of mutated Pol η and TTD-containing DNA versus TT-containing DNA is expressed as

$$\Delta\Delta G_{bind} = \Delta G_3 - \Delta G_4 = \Delta G_1 - \Delta G_2 \qquad (1)$$

The TI calculations were used to calculate ΔG_1 and ΔG_2, which in turn were used to calculate $\Delta\Delta G_{bind}$. The topologies were created including both λ end states containing Pol η, a DNA template−primer construct with a TTD or a TT in the template strand, and a dATP opposite the 3′T of the TTD/TT. The calculations were performed over three steps: first the charges on the TTD were removed, then the softcore van der Waals potential[41] was employed to transform the TTD to TT, and last the charges were resumed on the TT motif.

A comprehensive equilibration procedure was performed prior to data collection. Each system was energy-minimized for 25,000 steps at $\lambda = 0.5$ using the steepest descent method. Then, the minimized systems were equilibrated and simulated at λ values ranging from 0 to 1 with intervals of 0.1. Each system at a distinct λ value was heated during equilibration from 0 to 300 K over 200 ps of MD within the canonical ensemble (NVT) in the presence of a weak harmonic restraint on the solute. Then, the density of the system was allowed to adjust in an isobaric, isothermal ensemble (NPT) over 1 ns without any harmonic restraints utilizing Langevin dynamics with a collision frequency of 1.0 ps^{-1} to maintain a pressure of 1.0 bar and a temperature of 300 K. Subsequent to the NPT equilibration, a 5 ns production trajectory was propagated at each λ value within the NPT ensemble. Five independent cycles were calculated for each mutation using the same energy-minimized structures at $\lambda = 0.5$ but different initial velocities for the equilibration. The $\partial V/\partial\lambda$ data were gathered from these production MD trajectories at the discrete λ values every 2 ps. The average $\partial V/\partial\lambda$ values were plotted against the λ values, and the area under the emerging curve was calculated with the trapezoidal rule to obtain the free energy change for the reaction under investigation. The reported final relative binding free energy is the average of the numbers calculated in the five replicate thermodynamic cycles.

In the classical MD simulations, the local geometry optimization of the newly added side chains on residue 61 or 62 was followed by a gradual energy minimization performed on the entire systems. First, only the solvent atoms and the ions were energy-minimized, and then, the hydrogen atoms were energy-minimized. Subsequently, the side chains were energy-minimized by gradually weakening the harmonic positional restraints acting on them. Finally, the entire system was energy-minimized with no positional restraints. A total of 73,000 energy minimization steps were executed; 31,000 of these used the steepest descent method,[42] and the remaining 42,000 steps utilized the conjugate gradient method for minimization.[42] After the energy minimization, a two-stage equilibration MD protocol was carried out. First, the temperature was slowly raised from 0 to 300 K over 200 ps of MD within the canonical ensemble (NVT), while maintaining a weak harmonic restraint on the protein. Second, the harmonic restraints were removed, and an MD trajectory of 10 ns at 300 K was propagated at a constant pressure of 1.0 bar within an isobaric, isothermal ensemble (NPT) using Langevin dynamics with a collision frequency of 1.0 ps^{-1}.[43] Following this equilibration procedure, a trajectory was propagated for 1 μs for each system studied.

The MD trajectories were analyzed to elucidate the impact of the mutations applied to Pol η on the structure and equilibrium dynamics of the system. A comprehensive analysis of key

distances, root-mean-square deviations (RMSDs), root-mean-square fluctuations (RMSFs), and hydrogen-bonding interactions was conducted for each system. The relationship of the dATP and TTD/TT residues with the surrounding water molecules was also examined. These analyses were performed with the cpptraj utility of AmberTools14.[31]

3. RESULTS AND DISCUSSION

3.1. Enzyme Structure and Equilibrium Dynamics. To analyze the effects of these mutations on the structures and equilibrium motions of the enzyme, we propagated independent 1 μs MD trajectories on the TTD- and TT-containing systems. The RMSD fluctuations of Pol η in the mutant systems were similar to the fluctuations of the WT systems (Figure S2), except for a few jumps that were associated with the motions of solvent-exposed loops. The overall RMSF profiles of the mutant Pol η systems also did not exhibit significant differences from those of the WT systems, except for some variation in a solvent-exposed loop of the palm subdomain (Figure S3). The mobilities of the dATP and the TTD/TT regions were assessed individually through their RMSFs (Table S2). This analysis indicated that dATP has a comparable mobility in all mutant systems with or without the TTD and that this mobility is greater than the WT counterparts. The TTD and TT motifs also have greater mobilities in the mutant systems compared to the WT enzyme, with one exception. In addition, the TT motif has greater mobility than the TTD motif for the WT enzyme and the R61 mutants, but the reverse trend was observed for the S62 mutants.

3.2. Relative Binding Free Energies. In our previous study of WT Pol η, we found that binding of dATP to a Pol η•DNA complex with a TTD was thermodynamically favored over binding to this complex with a TT by 3.89 kcal/mol. This difference in binding free energies of dATP was attributed to more consistent Watson−Crick (WC) base pairing between the incoming dATP and the TTD, as well as to the greater extent of hydrogen-bonding interactions with the enzyme and the dATP for the TTD than for the two undamaged thymines (the TT). We hypothesized that the TTD was held more rigidly in place as a result of the more extensive hydrogen-bonding interactions between the TTD and the environment, which led to a more consistent and specific positioning of the lesion opposite the dATP. This more precise positioning could facilitate the tighter binding of dATP to the TTD than to the TT motif.[13]

As described above, herein we studied mutations of R61 and S62 by replacing these residues with their counterparts from Pol ι and Pol κ. We used TI to calculate the relative binding free energies of dATP to the Pol η•DNA complex with a TTD versus a TT (eq 1) for each of these mutant systems. The values are provided in Table 1. Negative values of $\Delta\Delta G_{bind}$ indicate that the binding of dATP to the TTD-containing system is thermodynamically favorable compared to the binding of dATP to the TT-containing system. The reported error bars were obtained from a statistical analysis of the five replicate runs performed for each system. Although the error bars are significant compared to the relative binding free energies themselves, the trends in the average relative binding free energies are meaningful in assessing the impact of the mutations on the specificity of the enzyme.

Table 1 indicates that the thermodynamic favorability for binding of dATP to the TTD-containing system compared to the TT-containing system is greater for the WT system than for

Table 1. Relative Free Energies of dATP Binding to the WT and Mutant Pol η•DNA Complexes for the DNA with a TTD versus a TT

system	$\Delta\Delta G_{bind}$[a]
WT	-3.89 ± 2.39
R61K	-1.27 ± 3.32
R61A	-0.82 ± 2.71
S62L	1.13 ± 3.45
S62A	-1.47 ± 2.67

[a]Negative value indicates that binding is thermodynamically more favorable for the TTD-containing system than for the TT-containing system, as given by eq 1.

any of the mutant systems. In other words, the ability of the enzyme to differentiate between TTD-containing and un-damaged DNA diminishes due to these mutations of R61 and S62. These calculations suggest that R61 and S62 play a key role in maintaining the specificity of Pol η for the TTD lesion compared to Pol ι or Pol κ, which are designed to counter other types of DNA lesions.

3.3. R61 Mutations: R61K and R61A. We examined the extent of WC base pairing between the 3′T of the TTD/TT and dATP in the MD simulations. Figure 1 depicts these base
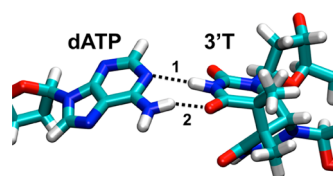
Figure 1. WC base pairing for the dATP and the 3′T of TTD. "1" is defined as the hydrogen bond in which the 3′T(N3) of the TTD/TT is the donor heavy atom, the hydrogen attached to it is the donor hydrogen, and the dATP(N1) is the acceptor. "2" is defined as the hydrogen bond in which the dATP(N6) is the donor heavy atom, the HN2 attached to it is the donor hydrogen, and the 3′T(O4) of the TTD/TT is the acceptor.

Table 2. Occurrences of the WC Base Pairing Interactions between the dATP and TTD/TT Motifs in the MD Trajectories for the WT and Mutant Pol η Systems

		occurrence[a]	
		H-bond 1[b]	H-bond 2[b]
WT	TTD	0.97	0.87
	TT	0.80	0.73
R61K	TTD	0.93	0.90
	TT	0.98	0.47
R61A	TTD	0.98	0.96
	TT	0.84	0.82
S62L	TTD	0.99	0.97
	TT	0.99	0.94
S62A	TTD	0.98	0.95
	TT	0.99	0.94

[a]The occurrence is defined as the fraction of saved configurations exhibiting this specific hydrogen bond, where a hydrogen bond is defined to have a heavy-atom donor−acceptor distance less than 3.5 Å and a donor−hydrogen−acceptor angle of 145−180°. [b]H-bonds 1 and 2 are defined in Figure 1.

pairing interactions, and Table 2 tabulates the occurrences of these hydrogen bonds in the MD trajectories. The WT and

R61A mutant systems maintained more consistent WC base pairing interactions between the incoming dATP and the 3′T of TTD relative to TT, which could contribute to the stronger binding affinities of dATP to TTD-containing systems. For the R61K mutant, however, the occurrence of the hydrogen bond between the 3′T(N3) of the TT and the dATP(N1) (labeled "1" in Figure 1) increased, while the occurrence of the hydrogen bond between the 3′T(O4) of the TT and the dATP(N6) (labeled "2" in Figure 1) significantly decreased compared to its WT counterpart. On the basis of this analysis, the differences in WC base pairing interactions cannot be used to explain the binding free energy differences between WT and these mutants. Furthermore, an analysis of the hydrogen bonding of the dATP molecule with the surrounding protein side chains shows very little difference between the TTD and TT systems in the presence of the R61 mutants. The most prevalent hydrogen bonds involving the side chains of Y52 and R55, as well as the backbone amides of C16, F17, and F18, are similar to our observations for the WT simulations.[12]

Mutating R to K partially diminishes the possible interactions of the side chain. Figure 2 depicts the multiple configurations of both side chains observed in the MD trajectories. The interactions between dATP, TTD/TT, and R61 or K61 are depicted in Figure 3. While hydrogen-bonding and cation−π interactions are still possible between K and dATP and the neighboring amino acids, the energetic benefits of the
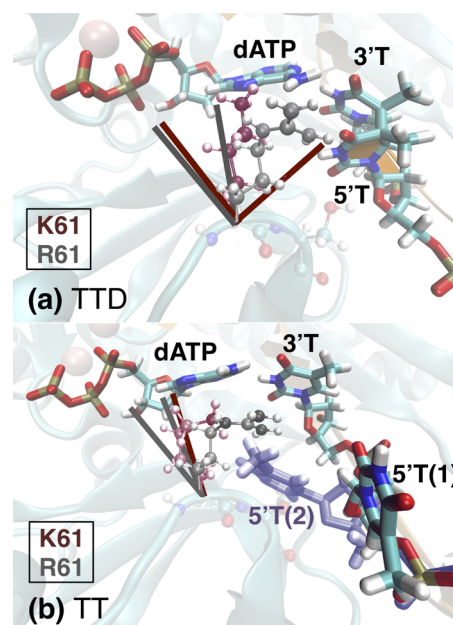
Figure 2. Relative positioning of dATP and residue 61 in the WT and R61K systems with a TTD (a) or a TT (b) motif. The WT R61 is shown in gray shades, and the mutant K61 is shown in burgundy shades, along with their matching-colored labels. For both R61 and K61, one configuration is depicted at atomic level in gray and burgundy, respectively, and the other two configurations are depicted as sticks that are oriented along the side chain. In part b, two dominant configurations of the 5′T of the TT motif are shown and are labeled as "5′T(1)" and "5′T(2)", where 5′T(2) is shown in blue shades. The R61 and K61 side chains adopt the conformations shown as sticks and at atomic level with the 5′T(1) conformation, while only the conformations shown as sticks are observed with the 5′T(2) conformation. The varying conformations of R61 were also observed in previous simulations.[24]
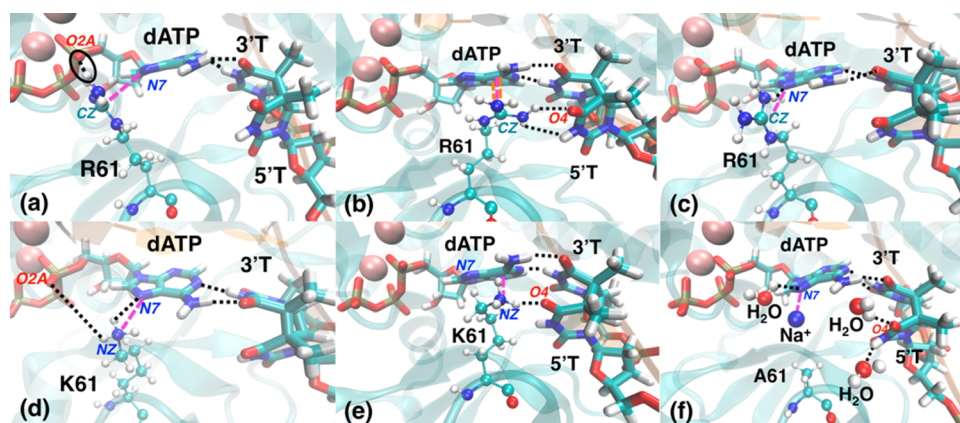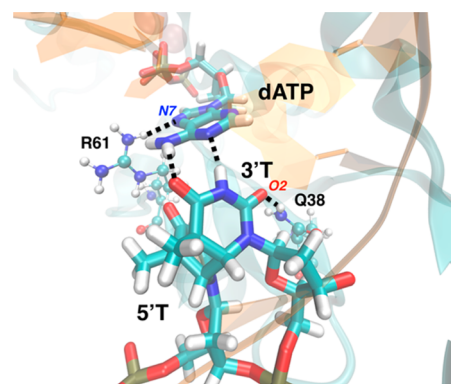
Figure 3. Hydrogen-bonding (black dashed lines), $\pi-\pi$ (orange dashed lines), and cation$-\pi$ (pink dashed lines) interactions of R61 or K61 with dATP and TTD. Each frame shows the WC base pairing interactions between the dATP and the 3′T of TTD as black dashed lines. (a) The guanidinium side chain of R61 interacts with one of the α-phosphate oxygens through charge−charge and hydrogen-bonding interactions (black dashed line, circled). This configuration displays a T-shaped $\pi-\pi$ (not indicated here) and a cation$-\pi$ (pinked dashed line) interaction between the R61 side chain and dATP(N7). (b) The guanidinium side chain of R61 interacts with the dATP base through $\pi-\pi$ (orange dashed lines) and cation$-\pi$ (pink dashed line, virtually indistinguishable from orange lines) interactions. This side chain configuration of R61 also allows hydrogen-bonding interactions with the 5′T of TTD (black dashed lines). (c) The guanidinium side chain of R61 interacts with the dATP(N7) through T-shaped $\pi-\pi$ (not indicated here), cation$-\pi$ (pink dashed line), and hydrogen-bonding (black dashed line) interactions. (d) The amine side chain of K61 interacts with the dATP(N7) through cation$-\pi$ (pink dashed line) and hydrogen-bonding (black dashed line) interactions. This side chain configuration of K61 also allows the formation of charge−charge and hydrogen-bonding interactions with one of the α-phosphate oxygens (black dashed line). (e) The amine side chain of K61 interacts with the dATP base through cation$-\pi$ interactions (pink dashed line). This side chain configuration of K61 also allows hydrogen-bonding interactions with the 5′T(O4) of TTD (black dashed line). (f) The A61 side chain opens up more room for incoming water and Na^+ ions in the active side, which compensate for the absence of a charged and bulky protein side chain. The hydrogen-bonding interactions between the dATP(N7) and nearby water, as well as 5′T of TTD and water, are shown as black dashed lines. A Na^+ ion comes into the active site occasionally and forms a cation$-\pi$ interaction with the dATP(N7) (pink dashed line).

interaction of two delocalized π systems, or $\pi-\pi$ interactions, are lacking for K but are present for R. The $\pi-\pi$ interactions are present for R but not for K because R contains a delocalized π system at the end of its side chain. Thus, this mutation removes the $\pi-\pi$ interactions between the base of dATP and R (orange dashed lines in Figure 3b), but it retains the cation$-\pi$ interactions (pink dashed lines in Figure 3a, b, c, d, e). Because the $\pi-\pi$ interactions between the base of dATP and R are missing with K, the TT motif is able to adopt a conformation in which the 3′T and 5′T stack with each other for the majority of the R61K mutant trajectory. In contrast, this stacked conformation is not sampled significantly in the WT trajectory because of steric hindrance arising from the $\pi-\pi$ interactions between the base of dATP and R. Furthermore, the K side chain is less bulky than the R side chain, and therefore, it samples a different set of configurations with respect to the dATP and the TTD/TT motifs. A more detailed analysis of these interactions and the associated distances is provided in the Supporting Information.

In contrast to the R61K mutation, the R61A mutation eliminates all of the possible hydrogen-bonding and cation$-\pi$ interactions with dATP and the 5′T of TTD/TT. The missing hydrogen bonding with residue 61 is efficiently replaced with hydrogen bonding to water molecules at both the dATP(N7) and the 5′T(O4) of TTD/TT (Figure 3f). In some instances of the R61A trajectory, a Na^+ ion from the solution is positioned within 3 Å of the dATP(N7) and compensates for the lacking cation$-\pi$ interaction at this site (Figure 3f and Figure S4).

3.3.1. Importance of Q38 and R61 for Positioning of dNTP and TTD/TT. Further analysis of the hydrogen-bonding patterns of the TTD/TT motifs revealed the importance of Q38 in the correct positioning of the TTD/TT for the nucleotidyl addition reaction by Pol η. R61 and Q38, the two evolutionarily

conserved residues in the Pol η enzymes across species, seem to act as clamps on the two sides of the base-paired dATP and 3′T of the TTD or TT in the active site, as shown in Figure 4 for

Figure 4. Hydrogen-bonding interactions between the side chain of Q38 and the 3′T(O2) of TTD and between the R61 side chain and the dATP(N7) are shown as black dashed lines. The WC base-pairing interactions between the 3′T of TTD and dATP are also shown as black dashed lines.

the TTD motif. R61 interacts with dATP and the TTD/TT, while Q38 interacts with the TTD/TT. Table 3 provides the occurrences of the Q38−TTD/TT hydrogen bonds in the MD trajectories. In the WT enzyme, Q38 does not appear to distinguish between the 3′Ts of the TTD and TT motifs. The contributions from the Q38−5′TTD/TT hydrogen bond might provide a slight advantage for the TTD. Note that the 5′T of the TTD is already locked into position after a consistent hydrogen bond is established with the 3′T, whereas the 5′T of the TT is more mobile and can expand into the bulk solvent,

Table 3. Occurrences of the Hydrogen Bonds Formed between the Q38 Side Chain Amide (NE2) and the 3′T(O2) or 5′T(O2) of the TTD/TT Motif in the MD Trajectories for the WT and Mutant Pol η Systems

	occurrence[a]			
	TTD		TT	
	3′T[b]	5′T	3′T	5′T
WT	0.47	0.19	0.46	0.00
R61K	0.29	0.04	0.14	0.71
R61A	0.47	0.09	0.31	0.00
S62L	0.35	0.13	0.79	0.00
S62A	0.54	0.47	0.56	0.97

[a]The occurrence is defined as the fraction of saved configurations exhibiting this specific hydrogen bond, where a hydrogen bond is defined to have a heavy-atom donor−acceptor distance less than 3.5 Å and a donor−hydrogen−acceptor angle of 145−180°. Some of the hydrogen bonds listed for the 3′ and 5′ thymines are bifurcated and therefore are reported in both the 3′T and 5′T columns. [b]The hydrogen bond to 3′T(O2) is depicted in Figure 4.

thereby precluding a hydrogen bond with Q38. In contrast to the WT enzyme, the relative occurrences of the Q38−TTD and Q38−TT hydrogen bonds indicate more consistent hydrogen-bonding interactions for the TT for all mutants except R61A if hydrogen bonds to both thymines of the TTD/TT motifs are considered.

For the R61K mutant, Q38 hydrogen bonds more consistently with TT than with TTD because it can interact better with the 5′T. Specifically, the Q38−3′TT and Q38−5′TT hydrogen bonds are observed in 14 and 71%, respectively, of the saved configurations, whereas the Q38−3′TTD and Q38−5′TTD hydrogen bonds are observed in 29 and 4%, respectively, of the saved configurations (Figure 4 and Table 3). The greater occurrence of the Q38−5′TT hydrogen bond compared to its TTD counterpart likely leads to a more rigid positioning of the TT, thereby facilitating dATP binding. Moreover, the DNA backbones of the TTD/TT motifs exhibit more consistent hydrogen-bonding interactions with the protein side chains through N324 and W64 for the TT motif than for the TTD motif (Table S4). The propensity of the TT motif to engage in more consistent hydrogen bonding with the enzyme in the R61K mutant decreases the binding free energy difference of dATP to the Pol η•TTD-containing DNA system versus the Pol η•TT-containing DNA system. These differences between the WT and R61K mutant hydrogen-bonding interactions, as well as the differences in cation−π and π−π interactions, provide an explanation for the relative binding free energy of $\Delta\Delta G_{bind}$ = −1.27 kcal/mol for the R61K mutant compared to the more negative $\Delta\Delta G_{bind}$ = −3.89 kcal/mol for the WT enzyme (Table 1).

In the R61A mutant, the Q38−TTD/TT hydrogen-bonding interactions are more consistent for the TTD, in contrast to the R61K mutant. Specifically, the Q38 side chain amide hydrogen bonds to the 3′T in 47% of the saved configurations for the TTD system and in 31% of the saved configurations for the TT system (Table 3). Thus, the variations in stabilization through Q38−TTD/TT hydrogen bonding do not explain the decreased binding free energy difference for the R61A mutant compared to the WT enzyme. In addition, no significant differences between the R61A and WT systems were observed in terms of the hydrogen-bonding interactions of dATP and TTD/TT to surrounding water molecules (Figures S6 and S7).

However, the hydrogen-bonding interactions between the TT motif and the protein surpass those between the TTD motif and the protein in terms of extent and consistency; in both cases, the dominant contributions arise from the interactions of the TTD/TT backbone with S62 and R371 (Table S5).

3.3.2. Na⁺ Ion Compensates for Lost Positive Charge in R61A. Another significant factor to consider is the compensation for the lost cation−π interactions as a result of the R61A mutation. The extended conformation of the 5′T of TT creates more space in the active site for a Na⁺ ion to be located near the N7 site of dATP in the TT-containing system. This Na⁺ ion provides an energetic advantage for TT because it allows a cation−π interaction at this site. A Na⁺ ion is observed consistently at this location for the R61A mutant but not for the wild-type enzyme or for the R61K mutant, suggesting that this pocket is negatively charged, thereby attracting a positive charge that may contribute to structural stability or possibly function. The radial distribution function for Na⁺ ions around the dATP(N7) indicates that Na⁺ is more prevalent for the R61A system with a TT-containing DNA compared to the R61A system with a TTD-containing DNA (Figure S8). The enhanced cation−π interaction between a Na⁺ ion and the TT compared to the TTD could decrease the difference between the binding free energies of dATP to the TT- and TTD-containing systems. Given that the guanidinium side chain of R61 occupies this site in the WT system, this difference in Na⁺ ion occupation for the R61A mutant provides a possible explanation for the relative binding free energy of $\Delta\Delta G_{bind}$ = −0.82 kcal/mol for the R61A mutant compared to the more negative $\Delta\Delta G_{bind}$ = −3.89 kcal/mol for the WT enzyme (Table 1).

3.4. S62 Mutations: S62L and S62A. The extent of WC base pairing between the 3′T of the TTD/TT and the dATP for both mutants is given in Table 2. The WC base pairing interactions for these entities in the S62 mutants are very consistent for both the TTD- and TT-containing systems. In contrast to the R61 mutant and WT systems, the S62 mutant systems do not exhibit a significant difference between the WC base pairing interactions of dATP and the 3′T of TTD versus TT. Compared to the more persistent base-pairing interactions for TTD versus TT in the WT system (Table 2), the lack of differentiation between the TTD and TT motifs in the S62 mutants is consistent with the less negative relative binding free energy, $\Delta\Delta G_{bind}$, for the S62 mutants compared to the WT enzyme. The hydrogen-bonding interactions of the dATP with the surrounding amino acids are not significantly different than those observed for the R61 mutants and the WT system. The backbone amides of C16, F17, and F18, along with the side chains of Y52 and R55, establish very consistent hydrogen bonds with the dATP, as in the R61 mutants and the WT systems.

The configurations adopted by the L62 side chain and its environment adjusting to these configurations are depicted in Figure 5. This figure also illustrates that the S62L mutation influences the motions of the adjacent R61 residue. The hydrogen-bonding, cation−π, and π−π interactions are not significantly different from their WT counterparts for the TTD systems. For the TT systems, however, the S62L system exhibits somewhat more consistent interactions than the WT system. In addition, the L62 side chain sterically inhibits movement of the R61 side chain toward the TTD/TT, which in turn strengthens the interactions between the R61 side chain and one of the α phosphate oxygens of the dATP for both the
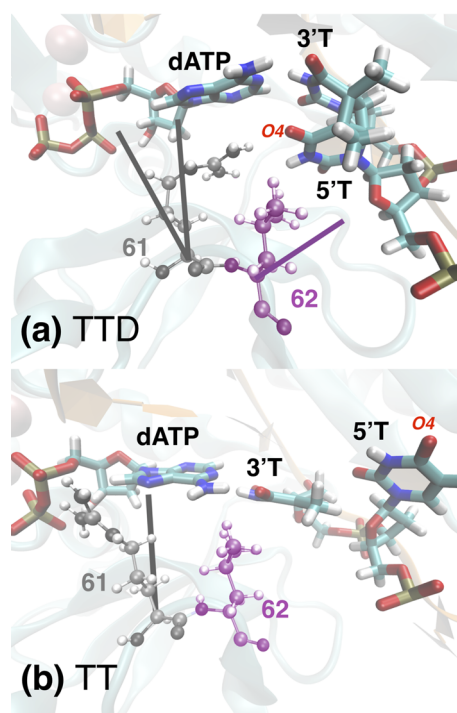
Figure 5. Relative positioning of dATP, R61, and L62 in the S62L systems with a TTD (a) or a TT (b) motif. The WT R61 is shown in gray shades, and the mutant L62 is shown in purple shades along with their matching-colored labels. For both R61 and L62, one configuration is depicted at atomic level in gray and purple, respectively, and the other configurations are depicted as sticks that are oriented along the side chain. In the presence of a TTD, the R61 side chain adopts three configurations, while the L62 side chain adopts only two. In the presence of a TT, both the R61 and L62 side chains each exhibit one less configuration compared to the system with a TTD. The extending 5′T of the TT is unable to interact effectively with the side chains of R61 and L62, resulting in the elimination of some configurations found in the presence of the TTD.

TTD and the TT (Figure 5), but especially for the TT after the 5′T of the TT moves away from the active site. In the WT system, such an interaction was observed in only 2% of the saved configurations from the TT trajectory, while this number increased to 47% in the S62L simulations. Similar behavior in terms of the R61 positioning was observed for the S62A TT-containing system.

Mutation of S62 to L results in the loss of the hydrogen bond between the S62(OG) and its closest TTD/TT hydrogen bond donor 5′T(O4). However, hydrogen-bonding interactions with water molecules partially compensate for this loss. In the S62L mutant complexed to a TT-containing DNA, the 5′T of the TT motif is oriented toward the bulk solvent, in the opposite direction from where it points within the TTD (Figure 5b). The bulkier L62 side chain may block the closer penetration of the 5′T into the active site, as observed with the R61K mutant complexed to the TT-containing DNA (Figure 2b, 5′T(2) in blue shading). The open conformation of the 5′T interacts strongly with residues from the little finger subdomain, mainly through π−π interactions and hydrogen bonds. This configuration is slightly more solvent exposed, as revealed in the total number of hydrogen bonds established between the TT motif and water molecules (Figure S8). We found that 94% of the saved configurations from the TT trajectory exhibited at least one hydrogen bond between the 5′T(O4) and a water

molecule. Hence, the loss of the S62 side chain hydrogen bond to this closest TTD/TT hydrogen bond donor was compensated effectively for TT. However, the TTD has more restricted mobility (Figure 5a), and the hydrophobic L62 side chain interferes with the passage of water molecules around 5′T(O4). This restriction results in a weaker compensation of the S62 side chain hydrogen bond by hydrogen bonds to water molecules: only 73% of the saved configurations displayed such an interaction. This better compensation of the stabilizing S62 side chain hydrogen bond for TT compared to TTD may factor into the more favorable binding of dATP to a TT rather than a TTD in the S62L mutant.

In the S62L mutant, the TT motif engages in more consistent hydrogen bonds not only with water but also with the surrounding amino acids. The Q38 side chain amide emerges as the most frequent hydrogen-bonding partner from the protein. The 3′T(O2) of the TT forms hydrogen bonds with the Q38 side chain in 79% of the saved configurations, while the TTD shows the analogous interaction in only 35% of the saved configurations (Table 3). On the basis of the analysis discussed above for the WT enzyme and the R61 mutants, hydrogen bonds involving Q38 appear to be significant for the stabilization of the TTD/TT motif, especially when the stability of dATP and TTD/TT is impaired with a mutation to a critical residue such as R61 or its neighbor. The higher occurrence of a hydrogen bond between Q38 and TT in the S62L mutant systems could favor dATP binding to TT over TTD. The enhanced hydrogen bonding of TT to both water and Q38, compared to the analogous hydrogen-bonding interactions of TTD, provides a possible explanation for the calculated positive value of the relative binding free energy. In particular, the relative binding free energy is $\Delta\Delta G_{bind}$ = 1.13 kcal/mol for the S62L mutant, favoring binding to the TT-containing system, compared to the value of $\Delta\Delta G_{bind}$ = −3.89 kcal/mol for the WT enzyme, favoring binding to the TTD-containing system (Table 1).

Similar to the S62L mutant, analysis of the hydrogen bonds around the TTD/TT motifs in the S62A mutant indicates that the TT motif establishes more consistent hydrogen bonds with the surrounding amino acids, particularly Q38, than the TTD motif. The Q38 side chain amide forms hydrogen-bonding interactions to 3′T(O2) and 5′T(O2) of both TTD and TT, but the interactions are more persistent for TT. For the TT-containing system, Q38 is hydrogen bonded to 3′T(O2) and 5′T(O2) in 56 and 97%, respectively, of the saved configurations (Table 3). Most of these hydrogen bonds are bifurcated, where the Q38 side chain hydrogen bonds to both of these acceptors simultaneously. For the TTD-containing system, Q38 is hydrogen bonded to 3′T(O2) and 5′T(O2) in 54 and 47%, respectively, of the saved configurations, and these hydrogen bonds are less likely to be bifurcated. Additionally, hydrogen bonding between the DNA backbone and the protein side chains is more prevalent at the TT motif compared to the TTD motif: the W64 side chain forms a hydrogen bond to the TT or TTD phosphate group with an occurrence of 84 or 22%, respectively. This hydrogen bond, combined with the one formed between the TTD/TT motif and Q38, provides greater stabilization to the TT motif, thereby decreasing the difference in the relative binding free energies of dATP to the TTD- or TT-containing systems with respect to WT. The differences between the WT and S62A mutant hydrogen-bonding interactions involving Q38 (Table 3), as well as other hydrogen-bonding interactions, provide a possible explanation

for the relative binding free energy of $\Delta\Delta G_{bind} = -1.47$ kcal/mol for the S62A mutant compared to the more negative $\Delta\Delta G_{bind} = -3.89$ kcal/mol for the WT enzyme (Table 1).

4. CONCLUSIONS

Mutations of R61 and S62 were found to decrease the difference between the binding free energy of dATP to a complex of Pol η•DNA with a TTD lesion versus without a TTD lesion. Although the calculated binding free energies are not quantitatively reliable, the trends are meaningful, especially in the context of the extensive analysis of the longer MD trajectories. The relative binding affinities arise from a complex interplay among interactions involving the dATP, the TTD/TT motif, and the enzyme side chains in the active site. The simulations illustrate that the mutations R61K, R61A, S62L, and S62A do not impact the global structure and equilibrium motions of Pol η. Instead, only local conformational changes around the mutation sites are observed. Moreover, the hydrogen-bonding interactions of the dATP molecule with the surrounding protein side chains are similar for the mutants and the WT for both the TTD- and TT-containing systems.

Analysis of the MD trajectories for the TTD- and TT-containing systems for the WT enzyme and the mutants provides insights into the molecular level basis for the changes in relative binding free energies of dATP to DNA with and without a TTD. Mutation of R61 to K results in different configurations for this side chain and alters the hydrogen-bonding, cation−π, and π−π interactions of this side chain with the dATP and the TTD/TT motif. The simulations also reveal that R61 and Q38 act as a clamp to position the dATP and TTD/TT in a manner conducive to the nucleotidyl addition reaction. Mutation of R61 to either K or A alters the balance among the complex interactions related to this clamp. Furthermore, mutation of R61 to A creates additional space in the active site that allows a Na$^+$ ion to be positioned near the dATP(N7) and engage in a π−cation interaction to partially compensate for the lost guanidinium from R61. This Na$^+$ ion is observed for the R61A mutant but not for the wild-type enzyme or for the R61K mutant, suggesting the possibility of a structural or functional role for a positive charge in this region. Mutation of S62 also affects R61 in a manner that influences its interactions with the dATP and the TTD/TT motif. Moreover, the S62L and S62A mutations eliminate hydrogen-bonding interactions between this side chain and the TTD/TT motif, although these interactions are often replaced by hydrogen bonding to water molecules, and indirectly influence interactions between Q38 and the TTD/TT motif.

All of these mutations alter the interactions within the active site in a manner that results in the binding free energies of dATP to the TTD- and TT-containing systems becoming more similar than they are for the WT system. As a result, these mutations are expected to decrease the ability of Pol η to distinguish between a TTD lesion and an undamaged DNA. This ability plays an important role in the specificity and effectiveness of this enzyme for bypassing TTD lesions during DNA replication. Understanding the basis for specificity is important for designing drugs to decrease the interference of this enzyme with platinum-based chemotherapy treatments.

■ ASSOCIATED CONTENT

Ⓢ Supporting Information

The Supporting Information is available free of charge on the ACS Publications website at DOI: 10.1021/acs.jpcb.6b09973.

Superimposed active sites of Pol η, Pol ι, and Pol κ; RMSD and RMSF profiles of WT and mutant Pol η systems; radial distribution functions for Na$^+$ ion in the R61A mutant systems; scatter distance plots for the WT and R61K mutant systems; hydrogen bond histograms for the R61A, S62L, and S62A mutant systems; comparisons of the individual active site residues of Pol η, Pol ι, and Pol κ; WC base-pairing interactions between dATP and TTD/TT motifs in WT and mutant systems; prevalent hydrogen bonds between the TTD/TT motifs and the R61 mutants; further analysis of R61 and K61 configurations (PDF)

■ AUTHOR INFORMATION

Corresponding Author

*E-mail: shs3@illinois.edu. Phone: 217-300-0335.

ORCID Ⓘ

Sharon Hammes-Schiffer: 0000-0002-3782-6995

Notes

The authors declare no competing financial interest.

■ REFERENCES

(1) Lange, S. S.; Takata, K.; Wood, R. D. DNA polymerases and cancer. *Nat. Rev. Cancer* **2011**, *11*, 96−110.

(2) Masutani, C.; Araki, M.; Yamada, A.; Kusumoto, R.; Nogimori, T.; Maekawa, T.; Iwai, S.; Hanaoka, F. Xeroderma pigmentosum variant (XP-V) correcting protein from HeLa cells has a thymine dimer bypass DNA polymerase activity. *EMBO J.* **1999**, *18*, 3491−3501.

(3) Yang, W.; Woodgate, R. What a difference a decade makes: Insights into translesion DNA synthesis. *Proc. Natl. Acad. Sci. U. S. A.* **2007**, *104*, 15591−15598.

(4) Cruet-Hennequart, S.; Gallagher, K.; Sokòl, A.; Villalan, S.; Prendergast, Á.; Carty, M. DNA polymerase η, a key protein in translesion synthesis in human cells. In *Genome Stability and Human Diseases*; Nasheuer, H.-P., Ed.; Springer: Dordrecht, The Netherlands, 2010; Vol. 50, pp 189−209.

(5) Yang, W. An overview of Y-family DNA polymerases and a case study of human DNA polymerase η. *Biochemistry* **2014**, *53*, 2793−2803.

(6) Kusumoto, R.; Masutani, C.; Shimmyo, S.; Iwai, S.; Hanaoka, F. DNA binding properties of human DNA polymerase η: Implications for fidelity and polymerase switching of translesion synthesis. *Genes Cells* **2004**, *9*, 1139−1150.

(7) McCulloch, S. D.; Kokoska, R. J.; Masutani, C.; Iwai, S.; Hanaoka, F.; Kunkel, T. A. Preferential cis-syn thymine dimer bypass by DNA polymerase η occurs with biased fidelity. *Nature* **2004**, *428*, 97−100.

(8) Matsuda, T.; Bebenek, K.; Masutani, C.; Hanaoka, F.; Kunkel, T. A. Low fidelity DNA synthesis by human DNA polymerase η. *Nature* **2000**, *404*, 1011−1013.

(9) Cruet-Hennequart, S.; Villalan, S.; Kaczmarczyk, A.; O'Meara, E.; Sokol, A. M.; Carty, M. P. Characterization of the effects of cisplatin and carboplatin on cell cycle progression and DNA damage response activation in DNA polymerase η-deficient human cells. *Cell Cycle* **2009**, *8*, 3043−3054.

(10) Parsons, J. L.; Nicolay, N. H.; Sharma, R. A. Biological and therapeutic relevance of nonreplicative DNA polymerases to cancer. *Antioxid. Redox Signaling* **2013**, *18*, 851−873.

(11) Ummat, A.; Rechkoblit, O.; Jain, R.; Choudhury, J. R.; Johnson, R. E.; Silverstein, T. D.; Buku, A.; Lone, S.; Prakash, L.; Prakash, S.; Aggarwal, A. K. Structural basis for cisplatin DNA damage tolerance by human polymerase η during cancer chemotherapy. *Nat. Struct. Mol. Biol.* **2012**, *19*, 628−632.

(12) Ucisik, M. N.; Hammes-Schiffer, S. Comparative molecular dynamics studies of human DNA polymerase η. *J. Chem. Inf. Model.* **2015**, *55*, 2672−2681.

(13) Ucisik, M. N.; Hammes-Schiffer, S. Relative binding free energies of adenine and guanine to damaged and undamaged DNA in human DNA polymerase η: Clues for fidelity and overall efficiency. *J. Am. Chem. Soc.* **2015**, *137*, 13240−13243.

(14) Makarova, A. V.; Kulbachinskiy, A. V. Structure of human DNA polymerase ι and the mechanism of DNA synthesis. *Biochemistry* **2012**, *77*, 547−561.

(15) Lior-Hoffmann, L.; Ding, S.; Geacintov, N. E.; Zhang, Y. K.; Broyde, S. Structural and dynamic characterization of polymerase κ's minor groove lesion processing reveals how adduct topology impacts fidelity. *Biochemistry* **2014**, *53*, 5683−5691.

(16) Lone, S.; Townson, S. A.; Uljon, S. N.; Johnson, R. E.; Brahma, A.; Nair, D. T.; Prakash, S.; Prakash, L.; Aggarwall, A. K. Human DNA polymerase κ encircles DNA: Implications for mismatch extension and lesion bypass. *Mol. Cell* **2007**, *25*, 601−614.

(17) Uljon, S. N.; Johnson, R. E.; Edwards, T. A.; Prakash, S.; Prakash, L.; Aggarwal, A. K. Crystal structure of the catalytic core of human DNA polymerase κ. *Structure* **2004**, *12*, 1395−1404.

(18) Vaisman, A.; Frank, E. G.; McDonald, J. P.; Tissier, A.; Woodgate, R. Pol ι-dependent lesion bypass in vitro. *Mutat. Res., Fundam. Mol. Mech. Mutagen.* **2002**, *510*, 9−22.

(19) Ishikawa, T.; Uematsu, N.; Mizukoshi, T.; Iwai, S.; Iwasaki, H.; Masutani, C.; Hanaoka, F.; Ueda, R.; Ohmori, H.; Todo, T. Mutagenic and nonmutagenic bypass of DNA lesions by drosophila DNA polymerases dpol η and dpol ι. *J. Biol. Chem.* **2001**, *276*, 15155−15163.

(20) Biertumpfel, C.; Zhao, Y.; Kondo, Y.; Ramon-Maiques, S.; Gregory, M.; Lee, J. Y.; Masutani, C.; Lehmann, A. R.; Hanaoka, F.; Yang, W. Structure and mechanism of human DNA polymerase η. *Nature* **2010**, *465*, 1044−1048.

(21) Su, Y.; Patra, A.; Harp, J. M.; Egli, M.; Guengerich, F. P. Roles of residues Arg-61 and Gln-38 of human DNA polymerase in bypass of deoxyguanosine and 7,8-dihydro-8-oxo-2-deoxyguanosine. *J. Biol. Chem.* **2015**, *290*, 15921−15933.

(22) Crowley, P. B.; Golovin, A. Cation-π interactions in protein-protein interfaces. *Proteins: Struct., Funct., Genet.* **2005**, *59*, 231−239.

(23) Gallivan, J. P.; Dougherty, D. A. Cation-π interactions in structural biology. *Proc. Natl. Acad. Sci. U. S. A.* **1999**, *96*, 9459−9464.

(24) Genna, V.; Gaspari, R.; Dal Peraro, M.; De Vivo, M. Cooperative motion of a key positively charged residue and metal ions for DNA replication catalyzed by human DNA polymerase η. *Nucleic Acids Res.* **2016**, *44*, 2827−2836.

(25) Genna, V.; Vidossich, P.; Ippoliti, E.; Carloni, P.; De Vivo, M. A self-activated mechanism for nucleic acid polymerization catalyzed by DNA/RNA polymerases. *J. Am. Chem. Soc.* **2016**, *138*, 14592−14598.

(26) Cornell, W. D.; Cieplak, P.; Bayly, C. I.; Gould, I. R.; Merz, K. M.; Ferguson, D. M.; Spellmeyer, D. C.; Fox, T.; Caldwell, J. W.; Kollman, P. A. A second generation force field for the simulation of proteins, nucleic acids, and organic molecules. *J. Am. Chem. Soc.* **1995**, *117*, 5179−5197.

(27) Cheatham, T. E.; Cieplak, P.; Kollman, P. A. A modified version of the Cornell et al. force field with improved sugar pucker phases and helical repeat. *J. Biomol. Struct. Dyn.* **1999**, *16*, 845−862.

(28) Perez, A.; Marchan, I.; Svozil, D.; Sponer, J.; Cheatham, T. E.; Laughton, C. A.; Orozco, M. Refinenement of the AMBER force field for nucleic acids: Improving the description of α/γ conformers. *Biophys. J.* **2007**, *92*, 3817−3829.

(29) Hornak, V.; Abel, R.; Okur, A.; Strockbine, B.; Roitberg, A.; Simmerling, C. Comparison of multiple AMBER force fields and development of improved protein backbone parameters. *Proteins: Struct., Funct., Genet.* **2006**, *65*, 712−725.

(30) Jorgensen, W. L.; Chandrasekhar, J.; Madura, J. D.; Impey, R. W.; Klein, M. L. Comparison of simple potential functions for simulating liquid water. *J. Chem. Phys.* **1983**, *79*, 926−935.

(31) Case, D. A.; Babin, V.; Berryman, J. T.; Betz, R. M.; Cai, Q.; Cerutti, D. S.; Cheatham, T. E., III; Darden, T. A.; Duke, R. E.; Gohlke, H.; et al. *AMBER 14*; University of California: San Francisco, CA, 2014.

(32) Allner, O.; Nilsson, L.; Villa, A. Magnesium ion-water coordination and exchange in biomolecular simulations. *J. Chem. Theory Comput.* **2012**, *8*, 1493−1502.

(33) Cieplak, P.; Cornell, W. D.; Bayly, C.; Kollman, P. A. Application of the multimolecule and multiconformational resp methodology to biopolymers - charge derivation for DNA, RNA, and proteins. *J. Comput. Chem.* **1995**, *16*, 1357−1377.

(34) Cornell, W. D.; Cieplak, P.; Bayly, C. I.; Kollman, P. A. Application of RESP charges to calculate conformational energies, hydrogen-bond energies, and free energies of solvation. *J. Am. Chem. Soc.* **1993**, *115*, 9620−9631.

(35) Ryckaert, J. P.; Ciccotti, G.; Berendsen, H. J. C. Numerical integration of the cartesian equations of motion of a system with constraints: Molecular dynamics of n-alkanes. *J. Comput. Phys.* **1977**, *23*, 327−341.

(36) York, D. M.; Darden, T. A.; Pedersen, L. G. The effect of long-range electrostatic interactions in simulations of macromolecular crystals - a comparison of the Ewald and truncated list methods. *J. Chem. Phys.* **1993**, *99*, 8345−8348.

(37) Pence, M. G.; Choi, J. Y.; Egli, M.; Guengerich, F. P. Structural basis for proficient incorporation of dTTP opposite o-6-methylguanine by human DNA polymerase ι. *J. Biol. Chem.* **2010**, *285*, 40666−40672.

(38) Irimia, A.; Eoff, R. L.; Guengerich, F. P.; Egli, M. Structural and functional elucidation of the mechanism promoting error-prone synthesis by human DNA polymerase κ opposite the 7,8-dihydro-8-oxo-2'-deoxyguanosine adduct. *J. Biol. Chem.* **2009**, *284*, 22467−22480.

(39) Gordon, J. C.; Myers, J. B.; Folta, T.; Shoja, V.; Heath, L. S.; Onufriev, A. H++: A server for estimating pk_as and adding missing hydrogens to macromolecules. *Nucleic Acids Res.* **2005**, *33*, W368−W371.

(40) Kaus, J. W.; Pierce, L. T.; Walker, R. C.; McCammon, J. A. Improving the efficiency of free energy calculations in the amber molecular dynamics package. *J. Chem. Theory Comput.* **2013**, *9*, 4131−4139.

(41) Steinbrecher, T.; Joung, I.; Case, D. A. Soft-core potentials in thermodynamic integration: Comparing one- and two-step transformations. *J. Comput. Chem.* **2011**, *32*, 3253−3263.

(42) Leach, A. R. *Molecular modelling: Principles and applications*, 2nd ed.; Pearson Education Limited: Essex, U.K., 2001.

(43) Allen, M. P.; Tildesley, D. J. *Computer simulations of liquids*; Clarendon Press: Oxford, U.K., 1987.